arXiv:cond-mat/0403425v1 [cond-mat.mes-hall] 17 Mar 2004

Multiphoton transitions in a macroscopic quantum two-state system

S. Saito,[1,2] M. Thorwart,[3] H. Tanaka,[1,2] M. Ueda,[1,2,4] H. Nakano,[1,2] K. Semba,[1,2] and H. Takayanagi[1,2]

[1]*NTT Basic Research Laboratories, NTT Corporation, Kanagawa 243-0198, Japan*
[2]*CREST, Japan Science and Technology Agency, Saitama 332-0012, Japan*
[3]*Institut für Theoretische Physik IV, Heinrich-Heine-Universität Düsseldorf, 40225 Düsseldorf, Germany*
[4]*Department of Physics, Tokyo Institute of Technology, Tokyo 152-8551, Japan*

We have observed multiphoton transitions between two macroscopic quantum-mechanical superposition states formed by two opposite circulating currents in a superconducting loop with three Josephson junctions. Resonant peaks and dips of up to three-photon transitions were observed in spectroscopic measurements when the system was irradiated with a strong RF-photon field. The widths of the multiphoton absorption dips are shown to scale with the Bessel functions in agreement with theoretical predictions derived from the Bloch equation or from a spin-boson model.

PACS numbers: 74.50.+r, 03.67.Lx, 42.50.Hz, 85.25.Dq

A macroscopic quantum two-state system (TSS) offers a unique testing ground for exploring the foundations of quantum mechanics [1]. This system can be in a quantum-mechanical superposition of macroscopically distinct states, and its quantum nature can be revealed by measuring the absorption of an integer number of photons from an externally applied photon field [2]. Since a macroscopic quantum system cannot be completely decoupled from its environment, dissipative and decoherence effects are unavoidable [1, 2, 3]. In addition to the investigation of fundamental physics, the quantum TSS also serves as an elementary carrier of information in a quantum information processor in the form of a quantum bit (qubit) [4]. Artificially designed superconducting circuits with mesoscopic Josephson junctions constitute an important class of macroscopic quantum systems. The charge degree of freedom of Cooper pairs is used to induce coherent quantum oscillations between two charge states of a Cooper pair box [5]. A circuit with a single relatively large Josephson junction, which is current-biased close to its critical current, forms a so-called Josephson phase qubit [6]. Moreover, three Josephson junctions arranged in a superconducting loop threaded by an externally applied magnetic flux constitute a flux qubit [7]. The device could be prepared in a quantum superposition of two states carrying opposite macroscopic persistent currents [8]. Coherent Rabi oscillations have been reported, when the qubit and the readout device are connected to obtain a large signal [9]. Rabi oscillations have also been observed in a system, where the qubit and the readout device are spatially separated [10]. Since these solid-state devices are thought to be scalable up to a large number of qubits, they are of particular interest in the context of solid-state quantum information processing [11].

The energy scale of quantum circuits containing Josephson junctions is in the microwave regime. This property was demonstrated in the current-voltage characteristics of a Josephson junction under microwave irradiation displaying the well-known Shapiro steps [12]. They appear at voltages corresponding to integer multiples of the applied microwave energy. With this phenomenon, the superconductor phase difference at the junction, which is a macroscopic degree of freedom, can be treated as a classical degree of freedom moving in the Josephson potential. In contrast, the quantum-mechanical behavior of the macroscopic phase difference was demonstrated using one-photon absorption processes between quantized energy levels within a single Josephson potential well [13]. Recently, Wallraff *et al.* presented experimental evidence of multiphoton absorption between quantized energy levels within the single potential well formed by a large current-biased Josephson junction [14]. In this Letter, we report the first observation of muliphoton transitions between superposition states of *macroscopically distinct states* [15], which are formed in the double-well potential system of a superconducting flux qubit. The presence of an energy gap at the degeneracy point of the macroscopically distinct states will be shown to be a prerequisite if we are to excite the qubit by applying a microwave even when the operating point is far from the degeneracy point.

Our device is fabricated by lithographic techniques that define the structure of an inner aluminum loop forming the qubit and an outer enclosing SQUID loop for the read-out (see Fig. 1(a)). They are spatially separated but magnetically coupled by the mutual inductance $M \simeq 7$ pH. The inner loop contains three Josephson junctions, one of which has an area $\beta(=0.7)$ times smaller than the nominally identical areas of the other two. The larger junctions have a Josephson energy of $E_{\rm J} = \hbar I_{\rm c}/2e$, where $I_{\rm c}$ is the critical current of the junction and e is the electron charge. The outer loop contains two Josephson junctions. By carefully designing the junction parameters [7, 8], the inner loop can be made to behave as an effective TSS [16]. In fact, the read-out result of the qubit changes greatly with the qubit design ranging from the purely classical to the quantum regime [17]. It is described by the Hamiltonian $\hat{H}_{\rm qb} = \frac{\hbar}{2}(\varepsilon_0\hat{\sigma}_z + \Delta\hat{\sigma}_x)$, where $\hat{\sigma}_{x,z}$ are the Pauli spin operators. Two eigenstates of $\hat{\sigma}_z$ are localized states $|\downarrow\rangle$ corresponding to the clockwise

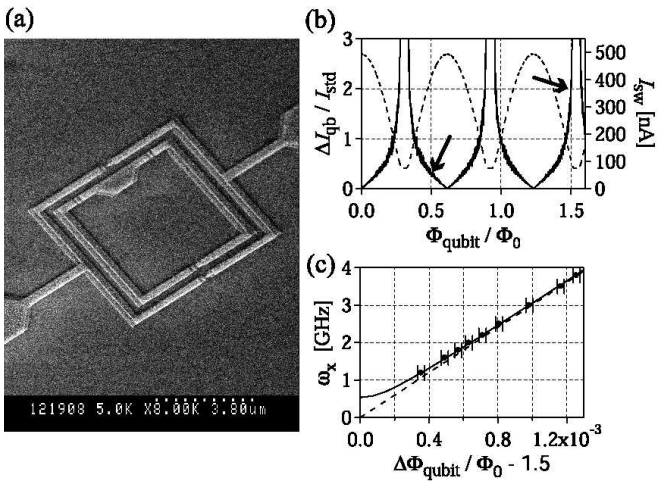


FIG. 1: (a) Scanning-electron-microscope picture of a superconducting flux qubit system. (b) Signal-to-noise ratio $\Delta I_{\rm qb}/I_{\rm std}$ (solid curve) and average switching current $I_{\rm sw}$ (dashed curve) as a function of applied flux through the qubit loop. The two arrows indicate the signal-to-noise ratios at $\Phi_{\rm qubit}/\Phi_0$=0.5 and 1.5. (c) Spectroscopic data of the qubit. Resonant frequency is plotted as a function of the half distance between the resonant peak and dip in $\Phi_{\rm qubit}/\Phi_0$. The solid curve represents a numerical fit to the data. The dashed line is the energy difference between localized states $|\downarrow\rangle$ and $|\uparrow\rangle$. From this fit, we obtained $E_{\rm J}/h$=380 [GHz] and $\Delta/2\pi$=0.56 [GHz].

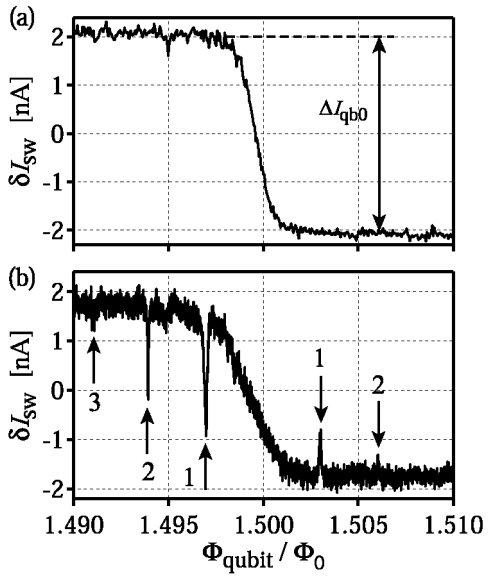


FIG. 2: Applied magnetic flux dependence of the qubit signal $\delta I_{\rm sw}$. We subtracted a sinusoidal background signal from the averaged switching current of the dc-SQUID $I_{\rm sw}$. (a) Without microwave irradiation. The data were obtained after averaging 2000 measurements. (b) With microwave irradiation. The data were obtained after averaging 500 measurements. The microwave power and frequency were 5 dBm at the generator and 9.1 GHz, respectively. Resonant peaks of up to two-photon processes and dips of up to three-photon processes were observed.

persistent current of the qubit and $|\uparrow\rangle$ corresponding to the counterclockwise current. Energy eigenstates $|0\rangle$ and $|1\rangle$ of $\hat{H}_{\rm qb}$ show energy anticrossing with energy gap $\hbar\Delta$. An externally applied static magnetic flux $\Phi_{\rm qubit}$ generates the energy imbalance $\hbar\varepsilon_0 = I_{\rm P}\Phi_0(\Phi_{\rm qubit}/\Phi_0 - f_{\rm op})$ between the two potential wells, where $\Phi_0 = h/2e$ is the flux quantum, $I_{\rm P} = I_{\rm c}\sqrt{1-(1/2\alpha)^2}$ is the persistent current of the qubit, and $f_{\rm op}$ is a qubit operating point which is a half integer. The effective energy gap in the biased qubit is $\hbar\Delta_{\rm b} = \hbar\sqrt{\varepsilon_0^2+\Delta^2}$. The qubit dynamics is controlled by a time-dependent RF field $s(t) = s\cos\omega_{\rm ex}t$ provided by an on-chip RF-line. This leads to an additional term in the Hamiltonian $\hat{H}_{\rm RF}(t) = -\frac{\hbar}{2}s(t)\hat{\sigma}_z$. If Δ is zero, $\hat{H}_{\rm qb} + \hat{H}_{\rm RF}(t)$ has only diagonal terms. In this case, the RF field cannot excite the qubit from the ground to the first excited state. A finite Δ is therefore a prerequisite for a spectroscopic experiment. In other words, resonant peaks and dips in the qubit signals are direct evidence for the coherent superposition of the macroscopically distinct states and for the multiphoton transitions to occur between them.

The qubit state was detected by measuring the switching currents of the dc-SQUID. We defined the switching current as the current when the I-V characteristic exceeded 30 μV. The probability distribution of the switching current was obtained by repeating the measurements typically 500 times. The measurements were carried out in a dilution refrigerator at a temperature of 30 mK. The bias voltage had a triangular waveform and was fed through large bias resistors of 1 MΩ to achieve a current-bias measurement. The sweep rate of the current was set at 120 μA/s and the frequency of the wave was 310 Hz. The RF line used to apply microwaves contained three attenuators in the input line: 30 dB at room temperature, 10 dB at 4.2 K and 10 dB at the base temperature. We fabricated an on-chip strip line to achieve strong coupling between the qubit and the RF line.

To achieve a good read-out resolution, we chose the operating point $f_{\rm op}$ at $\Phi_{\rm qubit}/\Phi_0$=1.5. Figure 1(b) shows the signal-to-noise ratio (S/N) $\Delta I_{\rm qb}/I_{\rm std}$ and the average switching current $I_{\rm sw}$ as functions of the applied flux through the qubit loop, where $I_{\rm std}$ denotes the standard deviation of the SQUID switching currents over 150 events, which may be considered to be a noise level in the qubit readout. The qubit signal amplitude $\Delta I_{\rm qb}$ should be proportional to the flux derivative of $I_{\rm sw}$, and this means that we can estimate $\Delta I_{\rm qb}$ by using the signal amplitude $\Delta I_{\rm qb0}$ at $\Phi_{\rm qubit}/\Phi_0$=1.5 (see Fig. 2(a)). In experiments, the qubit signal appears when $\Phi_{\rm qubit}/\Phi_0$ is a half-integer and the two arrows in Fig. 1(b) indicate the S/N at $\Phi_{\rm qubit}/\Phi_0$=0.5 and 1.5. Hence we chose the operating point at $\Phi_{\rm qubit}/\Phi_0$=1.5 to achieve a higher readout resolution.

Figure 2(a) shows the qubit signal $\delta I_{\rm sw}$ as a function of the external flux $\Phi_{\rm qubit}$ at $\Phi_{\rm qubit}/\Phi_0 \simeq 1.5$, which is derived by subtracting the sinusoidal background from the SQUID switching current $I_{\rm sw}$. It shows a change in the thermal averaged persistent current of the qubit. We obtained the sample temperature of 65 mK from a numerical fit to the data by using the qubit parameters $E_{\rm J}$ and Δ, which are derived from the spectroscopy measurements (see Fig. 1(c)). Figure 2(b) shows the $\Phi_{\rm qubit}$ dependence of the qubit signal under microwave irradiation. The observed distinct resonant peaks and dips are attributed to situations, in which the effective energy separation of the two qubit states $\Delta_{\rm b}$ matches an integer multiple of the RF photon energy $n\hbar\omega_{\rm ex}$. We have detected up to three resonant peaks and dips for various fixed RF frequencies. It should be noted that, at the resonant peaks and dips, the qubit is in a macroscopic quantum superposition of the two energy eigenstates.

The half width at half maximum (HWHM$_n$) and the normalized amplitude A_n of the dips are shown in Fig. 3(a) and (b) with various microwave amplitude $I_{\rm RF}$ for n=1, 2, 3, which is defined by $I_{\rm RF} = \exp[P_{\rm RF}/20]$. Here $P_{\rm RF}$ [dBm] is the microwave power at the signal generator. We derived the HWHM$_n$ and A_n from fitting the $\Phi_{\rm qubit}/\Phi_0$ dependence of $\delta I_{\rm sw}$ at around the resonant dips (see Fig. 2(b)) by using a Lorentzian with a linear background. The A_n values are normalized by the full amplitude of the dips (3 [nA]). The HWHM$_n$ carries important information on the dephasing and relaxation processes caused by the interaction with the environment. To calculate the line shape of the one-photon absorption dip, we have used phenomenological Bloch equations in the first approach. To describe the strong driving region and the n-th dip, we replace the single-photon Rabi frequency in the Bloch equations by the corresponding multi-photon frequency derived from theory of the dressed-atom approach [18]. This substitution has been verified by numerical simulations [19]. In a second approach, we have used a microscopic driven spin-boson model with a standard Ohmic spectral density [3, 20] to calculate the line-shape of the resonances. Both methods yield similar results in excellent agreement with the experimental ones as seen in Fig. 3(a).

The Bloch equations describe the dynamics of a spin $\frac{1}{2}$ in a constant field in the z-direction and a time-dependent field perpendicular to it. To keep the analogy between the spin $\frac{1}{2}$ and the flux qubit, we write the Hamiltonian in terms of the energy eigenstates [21] and obtain

$$\hat{H} = \frac{\hbar}{2}\left(\left\{\Delta_{\rm b} - \frac{\varepsilon_0}{\Delta_{\rm b}}s(t)\right\}\hat{\sigma}_z + \frac{\Delta}{\Delta_{\rm b}}s(t)\hat{\sigma}_x\right). \quad (1)$$

The second term of the Hamiltonian leads to a non-adiabatic periodic variation in the Larmor frequency. When $\frac{\varepsilon_0}{\Delta_{\rm b}}s \simeq \Delta_{\rm b}$, the Rabi frequency is decreased. However, we can disregard this term under the usual experimental condition, $\frac{\varepsilon_0}{\Delta_{\rm b}}s < \Delta_{\rm b}$. We have confirmed this by numerical simulations. If we adopt the rotating-wave approximation, the motion of the qubit spin $\langle\hat{\sigma}(t)\rangle$ in the laboratory frame can be described by the Bloch equations

$$\begin{aligned}\frac{d\langle\hat{\sigma}_{x/y}(t)\rangle}{dt} &= [\gamma\langle\hat{\sigma}(t)\rangle \times \vec{B}(t)]_{x/y} - \frac{\langle\hat{\sigma}_{x/y}(t)\rangle}{T_\phi},\\ \frac{d\langle\hat{\sigma}_z(t)\rangle}{dt} &= [\gamma\langle\hat{\sigma}(t)\rangle \times \vec{B}(t)]_z - \frac{\langle\hat{\sigma}_z(t)\rangle - \sigma_0}{T_{\rm r}}. \quad (2)\end{aligned}$$

Here, $\gamma\vec{B}(t) = -\frac{\hbar}{2}(\frac{\Delta}{2\Delta_{\rm b}}s\cos\omega_{\rm ex}t, \frac{\Delta}{2\Delta_{\rm b}}s\sin\omega_{\rm ex}t, \Delta_{\rm b})$, σ_0 is the thermal equilibrium value of $\langle\hat{\sigma}_z(t)\rangle$, and $T_{\rm r}$ and T_ϕ are the relaxation and dephasing times. The steady-state solutions of Eqs. (2) can be obtained in the rotating frame by setting $\frac{d\langle\hat{\sigma}_i(t)\rangle}{dt} = 0$. A resonant dip with a Lorentzian line shape appears at around $\omega_{\rm ex} \simeq \Delta_{\rm b}$. The HWHM$_1$ and the amplitude A_1 of the resonant dip follow as

$$\begin{aligned}{\rm HWHM}_1 &= \sqrt{\left(\frac{1}{T_\phi}\right)^2 + \omega_1^2\left(\frac{T_{\rm r}}{T_\phi}\right)^2}, \quad (3)\\ A_1 &= \frac{\omega_1^2 T_{\rm r}T_\phi}{1+\omega_1^2 T_{\rm r}T_\phi}\sigma_0, \quad (4)\end{aligned}$$

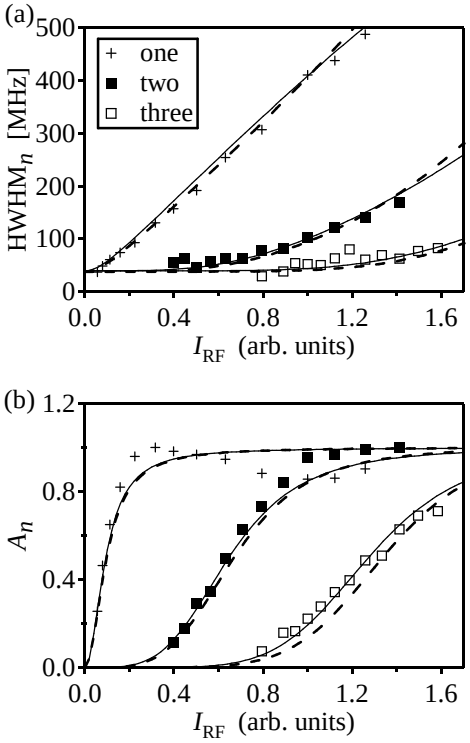


FIG. 3: Half width at half maximum (a) and normalized amplitude (b) of the resonant dips as functions of the microwave amplitude $I_{\rm RF}$. The microwave frequency is $\omega_x/2\pi = 3.8$ [GHz]. Solid (dashed) curves represent theoretical fits obtained by the Bloch equations combined with the dressed-atom approach (by the real-time path-integral method). We obtained $T_{\rm r1}$=31(27) [ns], $T_{\rm r2}$=84(66) [ns], $T_{\rm r3}$=430(240) [ns], T_ϕ=4.0(4.2) [ns], c=0.55(0.55). We have obtained similar results for $\omega_x/2\pi = 9.1$ [GHz] and 11.4 [GHz] (not shown).

where $\omega_1 = \frac{s\Delta}{2\Delta_b}$ is the Rabi frequency of the one photon absorption process.

To describe the regime of strong driving and n-photon absorption processes, we apply the dressed-atom aproach to the flux qubit. The Hamiltonian is given by $\hat{H} = \hat{H}_{qb} + \hbar\omega_{ex}a^\dagger a + g\hat{\sigma}_z(a + a^\dagger)$, where a and $a^\dagger$ are the annihilation and creation operators for a field mode with angular frequency ω_{ex} and g is a coupling constant between the qubit and the field. The Hamiltonian can be explicitly diagonalized when Δ=0. The eigenstates are given by $|\uparrow(\downarrow); N\rangle_{dressed} = \exp[-(+)g(a^\dagger - a)/\hbar\omega_{ex}]|\uparrow(\downarrow)\rangle|N\rangle$ and their eigenenergies are $E_N^{\uparrow(\downarrow)} = N\hbar\omega_{ex} - g^2/\hbar\omega_{ex} + (-)\frac{1}{2}\hbar\varepsilon_0$, where $|N\rangle$ are eigenstates of $\hbar\omega_{ex}a^\dagger a$. For $\Delta \ll \varepsilon_0$, first-order perturbation theory in the qubit Hamiltonian yields the term linear in Δ and when $n\hbar\omega_{ex} \simeq \hbar\Delta_b$, the two dressed states show anticrossing due to off-diagonal coupling $\frac{\hbar\Delta}{2}J_n(\alpha)$. Here, $J_n(\alpha)$ is the n-th order Bessel function of first kind and $\alpha \equiv 4g\sqrt{\langle N\rangle}/\hbar\omega_{ex}$ is the scaled amplitude of the driving field. If we prepare a localized initial state, Rabi oscillations occur with frequency $\omega_n = |\Delta|J_n(\alpha)$ [22].

We also applied a second approach starting from a microscopic driven spin-boson model with weak coupling to an Ohmic bath [3, 20]. In particular, we simplify the high-frequency approximation by numerically solving the pole equation (8) of Ref. [20]. We find that the solutions for the $n-$photon transition are given by $\theta = \theta_0$ and $\theta = \theta_n$. Inserting this in the expression for P_∞, we obtain an expression for the HWHM$_n$ similar to that in Eq. (3), where the phenomenological dephasing and relaxation times $T_{\phi/r}$ follow as the inverse of the weak-coupling rates of the spin-boson model [3]. This result differs slightly from that of the Bloch equations, which can be recovered by setting the field-dressed level spacing $\Delta_0 \equiv \Delta J_0(\alpha) \approx \Delta$ in the second approach.

To analyze HWHM$_n$ and A_n of the resonant dips, we substituted ω_n for Eqs. (3) and (4). We took T_{r1}, T_{r2}, T_{r3}, $T_{\phi n} = T_\phi$, and c as fitting parameters. Here T_{rn} and $T_{\phi n}$ are the relaxation and dephasing times related to the n-th photon absorption process. We defined a coupling constant c as $cI_{RF} = \alpha$. We found excellent agreement with the experimental data for both HWHM$_n$ and A_n (see Fig. 3). It should be noted that the relaxation and dephasing times T_{rn} and T_ϕ do not depend on the frequency of the corresponding multi-photon transition for a pure structure-less Ohmic environment (see also Eqs. (2)). This is no longer the case for a more complicated structured harmonic environment [23] as it is present in our device. Here, the plasmon frequency of the dc-SQUID provides an additional energy scale of the environment. Nevertheless, the global physics is captured by our simplified model.

In conclusion, we have reported on measurements of macroscopic superconducting circuits that reveal their quantum-mechanical behavior at low temperature. We have identified multiphoton transition processes in the qubit and found that the width of the n-photon resonance scales with the n-th Bessel function with its argument given as the ratio of the driving-field strength to the frequency of the photons. Our results add another example to the few cases of systems that exhibit clear quantum-mechanical behavior at a macroscopic scale.

We thank J. E. Mooij, C. J. P. M. Harmans, M. Grifoni, I. Chiorescu, Y. Nakamura, and D. Vion for useful discussions; T. Kutsuzawa for experimental help. This work has been suported by the CREST projiect of Japan Science and Technology Agency (JST).

[1] A. J. Leggett, in *Chance and Matter*, Lecture Notes of the Summer School of Theoretical Physics in Les Houches, Session XLVI, 1986, eds. J. Souletie, J. Vannimenus and R. Stora (North Holland, Amsterdam, 1987).
[2] M. Grifoni and P. Hänggi, Phys. Rep. **304**, 229 (1998).
[3] U. Weiss, *Quantum Dissipative Systems* (World Scientific, Singapore, 2nd ed., 1999).
[4] D. Bouwmeester, A. Ekert, and A. Zeilinger, *The Physics of Quantum Information* (Springer, Berlin, 2000).
[5] Y. Nakamura, and Y. A. Pashkin, J. S. Tsai, Nature **398**, 786 (1999); D. Vion, *et al.,* Science **296**, 886 (2002).
[6] Y. Yu, *et al.,* Science **296**, 889 (2002); J. M. Martinis, *et al.,* Phys. Rev. Lett. **89**, 117901 (2002).
[7] J. E. Mooij, *et al.,* Science **285**, 1036 (1999).
[8] C. H. van der Wal, *et al.,* Science **290**, 773 (2000).
[9] I. Chiorescu, *et al.,* Science **299**, 1869 (2003).
[10] H. Tanaka, S. Saito, T. Kutsuzawa, M. Ueda, H. Nakano, K. Semba, and H. Takayanagi, in preparation.
[11] Y. Makhlin, *et al.,* Rev. Mod. Phys. **73**, 357 (2001).
[12] S. Shapiro, Phys. Rev. Lett. **11**, 80 (1963); W. C. Danchi, *et al.,* Appl. Phys. Lett. **41**, 883 (1982).
[13] M. H. Devoret, *et al.,* Phys. Rev. Lett. **53**, 1260 (1984).
[14] A. Wallraff, *et al.,* Phys. Rev. Lett. **90**, 037003 (2003).
[15] A. J. Leggett, J. Phys. **14**, R415 (2002).
[16] H. Nakano, H. Tanaka, S. Saito, K. Semba, H. Takayanagi, and M. Ueda, in preparation.
[17] H. Takayangi, H. Tanaka, S. Saito, and H. Nakano, Phys. Scr. **T102**, 95 (2002); S. Saito, H. Tanaka, H. Nakano, M. Ueda, and H. Takayanagi, in *Quantum Computing and Quantum Bits in Mesoscopic Systems*, edited by A. J. Leggett, B. Ruggiero, and P. Silvestrini (Kluwer, New York, 2004), p. 161.
[18] C. Cohen-Tannoudji, J. Dupont-Roc, and G. Grynberg *Atom-Photon Interaction* (Wiley, New York, 1992).
[19] M. C. Goorden and F. K. Wilhelm, Phys. Rev. B **68**, 012508 (2003).
[20] L. Hartmann, *et al.,* Phys. Rev. E **61**, R4687 (2000).
[21] M. C. Goorden, Master's Thesis, (TU Delft, Delft, 2002).
[22] Y. Nakamura, Y. A. Pashkin, and J. S. Tsai, Phys. Rev. Lett. **87**, 246601 (2001).
[23] M. Thorwart, E. Paladino, and M. Grifoni, Chem. Phys. **296**, 333 (2004).